

## Detailed Topography of the Fermi Surface of $\text{Sr}_2\text{RuO}_4$

C. Bergemann,<sup>1</sup> S. R. Julian,<sup>1</sup> A. P. Mackenzie,<sup>2</sup> S. NishiZaki,<sup>3</sup> and Y. Maeno<sup>3,4</sup>

<sup>1</sup>*Cavendish Laboratory, University of Cambridge, Madingley Road, Cambridge CB3 0HE, United Kingdom*

<sup>2</sup>*School of Physics and Astronomy, University of Birmingham, Edgbaston, Birmingham B15 2TT, United Kingdom*

<sup>3</sup>*Department of Physics, Graduate School of Science, Kyoto University, Kyoto 606-8502, Japan*

<sup>4</sup>*CREST, Japan Science and Technology Corporation, Kawaguchi, Saitama 332-0012, Japan*

(Received 3 September 1999)

We apply a novel analysis of the field and angle dependence of the quantum-oscillatory amplitudes in the unconventional superconductor  $\text{Sr}_2\text{RuO}_4$  to map its Fermi surface (FS) in unprecedented detail and to obtain previously inaccessible information on the band dispersion. The three quasi-2D FS sheets not only exhibit very diverse magnitudes of warping, but also entirely different dominant warping *symmetries*. We use the data to reassess recent results on *c*-axis transport phenomena.

PACS numbers: 71.18.+y, 71.27.+a, 74.25.Jb

The layered perovskite oxide  $\text{Sr}_2\text{RuO}_4$  has attracted considerable experimental and theoretical attention since the discovery of superconductivity in this compound five years ago [1]. Fermi liquid behavior of several bulk transport and thermodynamic properties was observed in early work [1,2], and the existence of mass enhanced fermionic quasiparticles was demonstrated explicitly by the observation of quantum oscillations in the magnetization (de Haas–van Alphen or dHvA effect) and resistivity [3]. Quantitative similarities between the Fermi liquid in  $^3\text{He}$  and that in  $\text{Sr}_2\text{RuO}_4$  hint at the possibility of *p*-wave superconducting pairing [4]. Evidence supporting such a scenario has come from the existence of a very strong impurity effect [5], a temperature independent Knight shift into the superconducting state [6], a muon spin rotation study indicating broken time reversal symmetry [7], and a number of other experiments [8,9]. Taken together, these favor spin triplet superconductivity with a *p*-wave vector order parameter.

$\text{Sr}_2\text{RuO}_4$  appears to be an ideal material in which to investigate unconventional superconductivity in real depth: of all known compounds exhibiting this phenomenon,  $\text{Sr}_2\text{RuO}_4$  offers the best prospects of a complete understanding of the normal state properties within standard Fermi liquid theory [10]. This would provide a solid foundation for all theoretical models. It has become clear, however, that further progress will require very detailed knowledge of the electronic structure of  $\text{Sr}_2\text{RuO}_4$ . For example, one of the most successful current theories assumes that the Fermi surface (FS) consists of two sheets derived from bands with strong Ru  $d_{xz,yz}$  character and one with strong Ru  $d_{xy}$  character [11]. These are supposed to form weakly coupled subsystems with very different pairing interactions [12].

Of central importance to the understanding of  $\text{Sr}_2\text{RuO}_4$  is the origin of the quasiparticle mass enhancement and how it relates to magnetic fluctuations. Recent observations of cyclotron resonances [13] give the promise of separating the various contributions to the enhancement, but identifying the type of resonance and the extent to which electron interactions are affecting the observed masses re-

quires more detailed knowledge of the Fermi surface than has been available to date. Clues to the magnetic fluctuation spectrum have come from nuclear magnetic resonance [14] and neutron scattering experiments [15] and from calculations [16]. Both ferro- and antiferromagnetic fluctuations appear to be present, the latter due to nesting of the FS. Angle-dependent magnetoresistance oscillations (AMRO) can give information about the in-plane topography of the FS and the extent to which it is nested. However, with three bands crossing the Fermi level, the interpretation of AMRO data on  $\text{Sr}_2\text{RuO}_4$  [17] has been somewhat ambiguous.

Progress on all the issues discussed above requires high resolution, sheet-by-sheet knowledge of the FS of  $\text{Sr}_2\text{RuO}_4$ . As shown in previous studies [3], the dHvA effect is ideally suited to this, as data from individual FS sheets can be identified without ambiguity. For this reason, we have performed a comprehensive angular dHvA study in  $\text{Sr}_2\text{RuO}_4$ . Full analysis of the data required extension and generalization of previously reported theoretical dHvA treatments in quasi-2D materials [18]. As a result, we present an unprecedentedly detailed picture of the warping of each FS sheet, and we discuss the implications for electronic structure and *c*-axis transport.

Quantum-oscillatory effects in a crystal arise from the quantization of the cyclotron motion of the charge carriers in a magnetic field  $\mathbf{B}$ . For three-dimensional metals, only the extremal cyclotron orbits in  $\mathbf{k}$  space lead to a macroscopic magnetization, and the quantitative treatment has been known for decades [19].

For a quasi-2D metal, the FS consists of weakly corrugated cylinders. While such weak distortions have little effect on the cross-sectional areas which determine the dHvA frequency, they still affect the interference of the magnetization contributions of different parts of the FS and therefore lead to a characteristic amplitude reduction. Conversely, as we will show, analysis of the experimental dHvA amplitude behavior can reveal fine details of the topography of the underlying Fermi cylinders.

In the most basic case, a simple corrugation of the Fermi cylinder leads to a beat pattern in the magnetization. Analysis of the beats for on-axis fields gives some information about the *magnitude* of the warping, but further conclusions have to rely on assumptions about the precise form of the corrugation [3]. The *periodicity* of the FS dispersion can be determined within the traditional scope of the Yamaji effect [18,20]: the beat pattern has a characteristic dependence on the angle between the field and the cylinder axis. At a certain angle—the Yamaji angle—all FS cross sections have equal area to first order so that their magnetization contributions interfere constructively to a maximum amplitude without beats. A preliminary attempt to extract information on Sr<sub>2</sub>RuO<sub>4</sub> in this way, however, has not achieved agreement between the data and the predictions of the simple model [21]. We show that a much more extensive treatment is needed that (a) considers Fermi cylinder corrugation of arbitrary shape and (b) goes beyond the extremal orbit approximation on some sheets. Also, to extract meaningful information from experiments, one needs data of much higher quality than has been available to date.

In the following, we will briefly present the results of a full quantitative treatment of the oscillatory magnetization for a Fermi cylinder that is warped arbitrarily but is still compliant with the Brillouin zone (BZ) symmetry of Sr<sub>2</sub>RuO<sub>4</sub>; details will be presented elsewhere [22]. It is convenient to parametrize the corrugation of the cylinder through an expansion of the local Fermi wave vector,

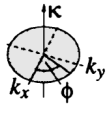
$$k_F(\phi, \kappa) = \sum_{\substack{\mu, \nu \geq 0 \\ \mu \text{ even}}} k_{\mu\nu} \cos \nu \kappa \begin{cases} \cos \mu \phi & (\mu \bmod 4 \equiv 0) \\ \sin \mu \phi & (\mu \bmod 4 \equiv 2) \end{cases} \quad (1)$$

(see Table I for illustration). Here,  $\kappa = ck_z/2$ , where  $c$  is the height of the body-centered tetragonal unit cell, and  $\phi$  is the azimuthal angle of  $\mathbf{k}$  in the  $(k_x, k_y)$  plane. The  $\beta$  and  $\gamma$  cylinders are centered in the BZ; symmetry allows nonzero  $k_{\mu\nu}$  only for  $\mu$  divisible by 4. The  $\alpha$  cylinder runs along the corners of the BZ and has nonzero  $k_{\mu\nu}$  only for  $\nu$  even and  $\mu$  divisible by 4, or for  $\nu$  odd and  $\mu \bmod 4 \equiv 2$ . The average Fermi wave vector is given by  $k_{00}$ , which is assumed to be much larger than the higher-order  $k_{\mu\nu}$ .

One also has to consider the effect of the magnetic field: spin splitting drives the spin-up and spin-down surfaces apart; the parameters  $k_{\mu\nu}$  can be taken to expand weakly and linearly in the field as in  $k_{\mu\nu}^{\uparrow} = k_{\mu\nu} \pm \chi_{\mu\nu} B$ . Ordinary spin splitting is described by  $\chi_{00}$  alone, while higher-order contributions would correspond to the underlying electronic band structure being flatter at some points on the Fermi surface than at others. Indeed, this anomalous spin splitting will prove essential for describing the  $\alpha$  sheet in Sr<sub>2</sub>RuO<sub>4</sub>.

If a magnetic field is applied at polar and azimuthal angles  $\theta$  and  $\phi$ , the Fermi surface cross-sectional area perpendicular to the field which cuts the cylinder axis at  $\kappa$  is given to first order by the Bessel function expansion

TABLE I. Summary of the extracted warping parameters  $k_{\mu\nu}$  (in units of  $10^7 \text{ m}^{-1}$ ) of the three FS sheets of Sr<sub>2</sub>RuO<sub>4</sub> [23]. Entries symbolized by a long dash are forbidden by the BZ symmetry. The first row visualizes the warping for the different values of  $\mu$  and  $\nu$ , on top of a large  $k_{00}$ .

						
	$k_{00}$	$k_{01}$	$k_{02}$	$k_{21}$	$k_{41}$	$k_{42}$
$\alpha$	305	—	-0.33	1.3	—	1.0
$\beta$	623	3.9	small	—	-1.9	small
$\gamma$	754	small	0.5	—	small	0.3

$$a^{\uparrow\downarrow}(\kappa) = \frac{\pi(k_{00}^{\uparrow\downarrow})^2}{\cos \theta} + \frac{2\pi k_{00}}{\cos \theta} \sum_{\substack{\mu \geq 0, \nu \geq 1 \\ \mu \text{ even}}} k_{\mu\nu}^{\uparrow\downarrow} J_{\mu}(\nu \kappa_F \tan \theta) \\ \times \cos \nu \kappa \begin{cases} \cos \mu \phi & (\mu \bmod 4 \equiv 0) \\ -\sin \mu \phi & (\mu \bmod 4 \equiv 2) \end{cases} \quad (2)$$

which is a generalization of Yamaji's earlier treatment [18]; here,  $\kappa_F = ck_{00}/2$ . The total quantum oscillatory magnetization now arises from the interference of the individual contributions of the cylinder cross sections; at constant chemical potential, the fundamental component of the oscillations is given by

$$\tilde{M} \propto \sum_{\uparrow\downarrow} \int_0^{2\pi} d\kappa \sin\left(\frac{\hbar a^{\uparrow\downarrow}(\kappa)}{eB}\right). \quad (3)$$

Equations (2) and (3) describe oscillations at the undistorted frequency  $\hbar k_{00}^2/2e \cos \theta$ , with a characteristic amplitude modulation induced by the interference. One can thus infer the warping parameters  $k_{\mu\nu}$  by modeling experimentally obtained amplitude data [23].

We have performed a thorough dHvA rotation study in the  $[001] \rightarrow [110]$  plane on a high-quality crystal of Sr<sub>2</sub>RuO<sub>4</sub> with  $T_c > 1.3$  K. The experiments were carried out on a low noise superconducting magnet system in field sweeps from 16 to 5 T, at temperatures of 50 mK. A modulation field of 5.4 mT amplitude was applied to the grounded sample, and the second harmonic of the voltage induced at a pickup coil around the sample was recorded, essentially measuring  $\partial^2 M / \partial B^2$ , with well-established extra contributions from the field modulation, impurity scattering, and thermal smearing [19].

A typical signal trace, demonstrating the high quality of our data, can be viewed in Fig. 1. Overall, 35 such sweeps were performed, at angular intervals of  $2^\circ$ . The oscillations from the three FS sheets are well separated in frequency, and for each we extracted the field dependent dHvA amplitude by filtering in the Fourier domain. The dHvA amplitude can then be visualized versus magnitude and direction of the field, as shown in the density plot in Fig. 2 for the  $\alpha$  sheet. We have also performed similar

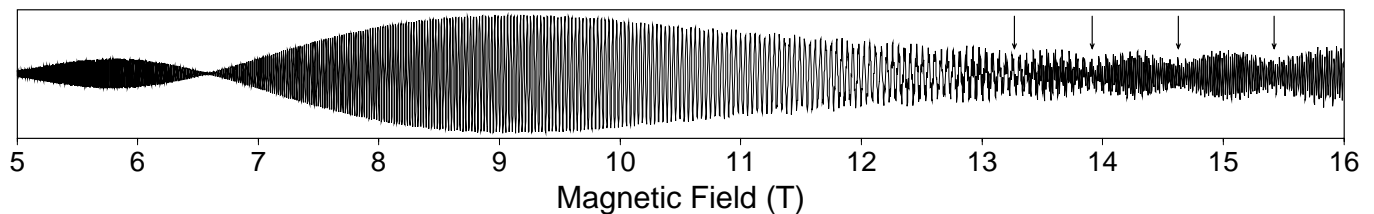


FIG. 1. Example of a dHvA field sweep on  $\text{Sr}_2\text{RuO}_4$ , for  $\theta = 9.8^\circ$  off the  $c$  axis in the  $[001] \rightarrow [110]$  rotation study. The vertical axis is the pickup signal (in arbitrary units) at the second harmonic of the excitation frequency. At high fields, beats in the  $\beta$  oscillations are visible, as indicated by arrows.

data analysis for a second extensive rotation study of short high-field (18 to 15 T) sweeps in the  $[001] \rightarrow [100]$  plane; these runs used a different sample. We now turn to the results of the analysis for all three FS sheets, where Table I presents the deduced values for the  $k_{\mu\nu}$ .

*$\alpha$  sheet.*—The most striking features of the data in Fig. 2 are qualitative differences with similar data in the  $[001] \rightarrow [100]$  plane (Ref. [21] and the present study), and the absence of spin zeros that should be visible as vertical black lines. We are able to account for both effects, and produce near-perfect agreement with experiments as seen by comparing the two panels of Fig. 2, using the  $k_{\mu\nu}$  as given in Table I. The dominant  $k_{21}$  term affects the dHvA amplitude for  $\phi = 45^\circ$  but has no effect for fields in the  $[001] \rightarrow [100]$  plane. The absence of spin zeros arises from the presence of a finite  $\chi_{21} \approx -5 \times 10^5 \text{ m}^{-1} \text{ T}^{-1}$  in addition to  $\chi_{00} = 10.4 \times 10^5 \text{ m}^{-1} \text{ T}^{-1}$ . The same parameters account equally well for data from  $[001] \rightarrow [100]$  rotations and for the amplitude of the second harmonic for both rotation directions. It should be noted that the warping of the  $\alpha$  cylinder is so weak—at some angles and fields it is smaller than the Landau level spacing—that the success of the model requires the use of our exact treatment beyond the extremal orbit approximation.

*$\beta$  sheet.*—The warping is comparatively large, and the extremal orbit approximation is valid over most of the angular range. The Yamaji angle of  $32^\circ$  and the variation of the (relatively fast) beat frequency  $\Delta F$  with  $\theta$  (Fig. 3) reveal that the dominant warping parameters are  $k_{01}$  and  $k_{41}$ , as tabulated in Table I. They have opposite

signs, so the  $c$ -axis dispersion is *largest along the zone diagonals*. It is difficult to extract meaningful information on the higher-order terms, but we believe that the data set an upper bound for a double warping contribution of  $|k_{02}| < 10^7 \text{ m}^{-1}$ . The spin-splitting behavior is intricate, and while it is certain that higher-order  $\chi_{\mu\nu}$  are needed to explain the data, it is impossible at this stage to extract them without ambiguity.

*$\gamma$  sheet.*—Because of stronger impurity damping, the  $\gamma$  signal is observable only at fields of more than 13 T. Along  $[001] \rightarrow [110]$ , its amplitude peaks at  $\theta = \pm 13.7^\circ$ , implying that the dominant corrugation is *double warping*, i.e.,  $k_{02} \gg k_{01}$ . We obtained a rough estimate of its strength from the *sharpness* of this amplitude maximum; it is difficult to assess  $k_{02}$  from an on-axis beat pattern, as that cannot be established in the short field range over which  $\gamma$  oscillations are visible. For the  $[001] \rightarrow [100]$  rotation, the amplitude maximum occurs at  $\theta = 14.6^\circ$ . The deviation of the two measured  $\theta$  values from each other and from the simple Yamaji prediction of  $14.1^\circ$  yields  $k_{42}$ , whose sign implies that the  $c$ -axis dispersion is *largest along the zone axes*. At present, it is not possible to extract reliable information on the spin-splitting parameters.

To the order of expansion given here, the semiclassical contribution of each FS sheet to the  $c$ -axis conductivity can be calculated from  $\sigma_{zz} \propto k_{00} \sum \nu^2 (1 + \delta_{\mu 0}) k_{\mu\nu}^2$ . The  $\beta$  sheet dominates with a 86% share, compared to 8% for the  $\alpha$  and 6% for the  $\gamma$  sheet. This provides new insight into recent AMRO experiments by Ohmichi *et al.* [17] as it strongly suggests that the AMRO signal originates

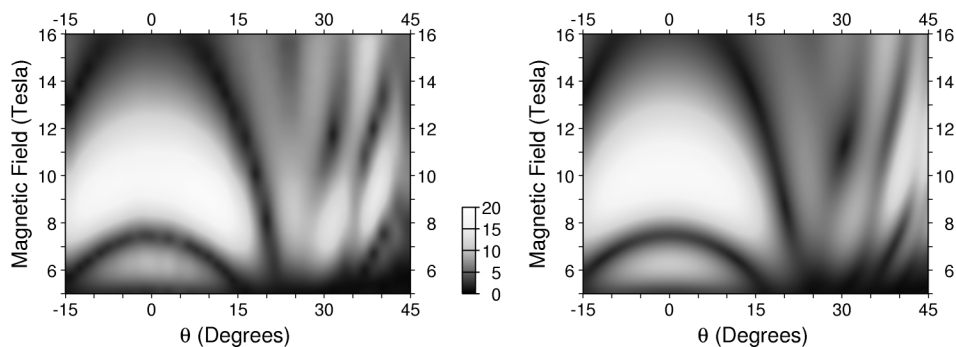


FIG. 2. Density plot of the field-dependent dHvA amplitude (in arbitrary units) of the  $\alpha$  frequency in  $\text{Sr}_2\text{RuO}_4$ , in the experimental  $[001] \rightarrow [110]$  rotation study (left), and comparison with the theoretical simulation, using the warping parameters in Table I (right). The theoretical calculation incorporates experimental effects such as the field modulation amplitude characteristic.

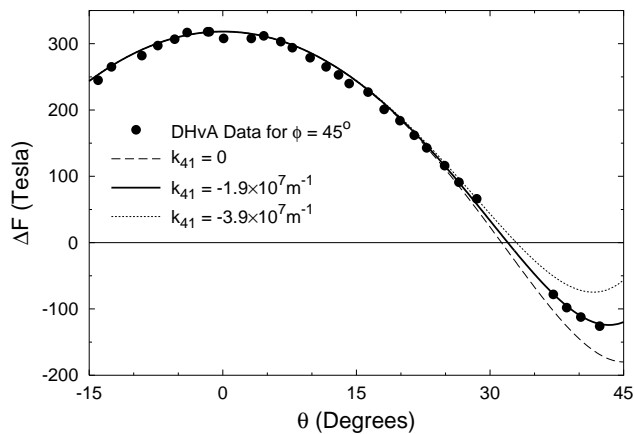


FIG. 3. Angular dependence of the beat frequency of the  $\beta$  oscillations in  $\text{Sr}_2\text{RuO}_4$  (cf. Fig. 1) in the  $[001] \rightarrow [110]$  rotation study (full circles).  $\Delta F(0^\circ)$  fixes  $k_{01}$  at  $3.9 \times 10^7 \text{ m}^{-1}$ ; the data are compared against the predicted behavior for cylindrically symmetric warping (dashed line), for zero dispersion along the BZ axes (dotted line), and for  $k_{04}$  as tabulated in Table I (solid line).

predominantly from the  $\beta$  sheet (rather than the  $\alpha$  sheet as had previously been assumed). The AMRO data then fix the “squareness” parameter of the  $\beta$  cylinder as  $k_{40} = -5.3 \times 10^8 \text{ m}^{-1}$ , giving quantitative information about the FS nesting on that sheet.

High-precision dHvA can also provide normally inaccessible information on spin-dependent many-body effects, by measuring both the specific heat and the spin susceptibility mass enhancements. For the  $\alpha$  sheet, we have  $m^*/m = 3.4$  and  $m_{\text{susc}}^*/m = 4.1$ , the latter obtained from spin-splitting analysis assuming  $g \approx 2$ . We would expect the ratio  $m_{\text{susc}}^*/m^*$  to diverge at a ferromagnetic quantum critical point; the small ratio here suggests that, at least for the  $\alpha$  sheet, the paramagnetic susceptibility enhancement is matched by specific heat contributions from phonons or large- $q$  spin fluctuations [10,15].

Finally, an intriguing feature of the present study is the qualitative difference between the dominant warping symmetries observed for the three FS sheets of  $\text{Sr}_2\text{RuO}_4$ . Detailed comparison with the results of band structure calculations would be very informative to test the accuracy of these computations for the weak out-of-plane dispersions in quasi-2D metals in general. An outstanding puzzle in the cuprates, for example, is that such calculations generally overestimate the  $c$ -axis coupling, motivating theories of 2D confinement. For  $\text{Sr}_2\text{RuO}_4$ , in particular, the  $\gamma$  sheet displays (a) small and (b) double warping, indicating that (a) its orbital character is mainly in-plane, i.e., Ru  $d_{xy}$ , and (b) the dominant  $c$ -axis transport mechanism for the  $d_{xy}$  orbitals is hopping to the *next-nearest* RuO<sub>2</sub> layer.

In summary, the full analysis of angle-dependent dHvA amplitude data has emerged as an extremely powerful tool

to determine the exact topography of the FS in quasi-2D metals. We have been able to extract quantitative information on the corrugation of all three Fermi cylinders of  $\text{Sr}_2\text{RuO}_4$ . The single warping of the  $\beta$  sheet provides most of the  $c$ -axis dispersion, while the ellipsoidal warping of the  $\alpha$  sheet and the double warping of the  $\gamma$  sheet are less significant.

We thank S. Hill, E. M. Forgan, A. J. Schofield, G. J. McMullan, and G. G. Lonzarich for stimulating and fruitful discussions. The work was partly funded by the U.K. EPSRC. C. B. acknowledges the financial support of Trinity College, Cambridge; and A. P. M. gratefully acknowledges the support of the Royal Society.

- 
- [1] Y. Maeno *et al.*, Nature (London) **372**, 532 (1994).
  - [2] Y. Maeno *et al.*, J. Phys. Soc. Jpn. **66**, 1405 (1997).
  - [3] A. P. Mackenzie *et al.*, Phys. Rev. Lett. **76**, 3786 (1996); the correct quasiparticle masses are given in A. P. Mackenzie *et al.*, J. Phys. Soc. Jpn. **67**, 385 (1998).
  - [4] T. M. Rice and M. Sigrist, J. Phys. Condens. Matter **7**, 643 (1995).
  - [5] A. P. Mackenzie *et al.*, Phys. Rev. Lett. **80**, 161 (1998).
  - [6] K. Ishida *et al.*, Nature (London) **396**, 658 (1998).
  - [7] G. M. Luke *et al.*, Nature (London) **394**, 558 (1998).
  - [8] K. Ishida *et al.*, Phys. Rev. B **56**, 505 (1997).
  - [9] R. Jin *et al.*, Phys. Rev. B **59**, 4433 (1999); C. Honerkamp and M. Sigrist, Prog. Theor. Phys. **100**, 53 (1998).
  - [10] S. R. Julian *et al.*, Physica (Amsterdam) **261B**, 928 (1999).
  - [11] T. Oguchi, Phys. Rev. B **51**, 1385 (1995).
  - [12] D. F. Agterberg, T. M. Rice, and M. Sigrist, Phys. Rev. Lett. **78**, 3374 (1997).
  - [13] S. Hill *et al.*, cond-mat/9905147, Phys. Rev. Lett. (to be published).
  - [14] T. Imai *et al.*, Phys. Rev. Lett. **81**, 3006 (1998); H. Mukuda *et al.*, J. Phys. Soc. Jpn. **67**, 3945 (1998).
  - [15] Y. Sidis *et al.*, Phys. Rev. Lett. **83**, 3320 (1999).
  - [16] I. I. Mazin and D. J. Singh, Phys. Rev. Lett. **79**, 733 (1997).
  - [17] E. Ohmichi *et al.*, Phys. Rev. B **59**, 7263 (1999).
  - [18] K. Yamaji, J. Phys. Soc. Jpn. **58**, 1520 (1989).
  - [19] See, for example, D. Shoenberg, *Magnetic Oscillations in Metals* (Cambridge University Press, Cambridge, England, 1984).
  - [20] See, for example, J. Wosnitza, *Fermi Surfaces of Low-Dimensional Organic Metals and Superconductors* (Springer, Berlin, 1996).
  - [21] Y. Yoshida *et al.*, J. Phys. Soc. Jpn. **67**, 1677 (1998).
  - [22] C. Bergemann *et al.* (to be published).
  - [23] The dHvA effect is insensitive to  $k_{\mu 0}$  for  $\mu > 0$ ; these parameters can be probed only by other methods such as AMRO. Ambiguities can also arise for the *sign* of the  $k_{\mu\nu}$ : while the average Fermi wave vector  $k_{00}$  and the spin-splitting  $\chi_{00}$  must be positive, the dHvA amplitude is invariant under a simultaneous sign change of all other  $k_{\mu\nu}$ , or of both  $k_{\mu\nu}$  and  $\chi_{\mu\nu}$  for all odd  $\nu$ .